AGU PUBLICATIONS

JGR

Journal of Geophysical Research: Space Physics

RESEARCH ARTICLE
10.1002/2013JA019728

Key Points:
- The strong Psw compression intensifies dayside and nightside reconnection rates
- Dayside reconnection contributes more to the CPCP increase during southward IMF
- Dayside contribution weakens during northward IMF due to the lobe reconnection

Correspondence to:
H. K. Connor,
hyunju.connor@cosmiac.org;
hyunjuconnor@gmail.com

Citation:
Connor, H. K., E. Zesta, D. M. Ober, and J. Raeder (2014), The relation between transpolar potential and reconnection rates during sudden enhancement of solar wind dynamic pressure: OpenGGCM-CTIM results, *J. Geophys. Res. Space Physics*, *119*, 3411–3429, doi:10.1002/2013JA019728.

Received 24 DEC 2013
Accepted 16 APR 2014
Accepted article online 23 APR 2014
Published online 9 MAY 2014

The relation between transpolar potential and reconnection rates during sudden enhancement of solar wind dynamic pressure: OpenGGCM-CTIM results

H. K. Connor[1,3], E. Zesta[2], D. M. Ober[3], and J. Raeder[4]

[1]Configurable Space Microsystems Innovations and Applications Center, University of New Mexico, Albuquerque, New Mexico, USA, [2]NASA Goddard Space Flight Center, Greenbelt, Maryland, USA, [3]Air Force Research Laboratory, Kirtland AFB, Albuquerque, New Mexico, USA, [4]Space Science Center, University of New Hampshire, Durham, New Hampshire, USA

Abstract This study investigates how solar wind energy is deposited into the magnetosphere-ionosphere system during sudden enhancements of solar wind dynamic pressure (P_{sw}), using the coupled Open Geospace General Circulation Model–Coupled Ionosphere Thermosphere Model (OpenGGCM-CTIM) 3-D global magnetosphere-ionosphere-thermosphere model. We simulate three unique events of solar wind pressure enhancements that occurred during negative, near-zero, and positive interplanetary magnetic field (IMF) B_z. Then, we examine the behavior of the dayside and nightside reconnection rates and quantify their respective contributions to cross polar cap potential (CPCP), a proxy of ionospheric plasma convection strength. The modeled CPCP increases after a P_{sw} enhancement in all three cases, which agrees well with observations from the Defense Meteorological Satellite Program spacecraft and predictions from the assimilative mapping of ionospheric electrodynamics technique. In the OpenGGCM-CTIM model, dayside reconnection increases within 9–13 min of the pressure impact, while nightside reconnection intensifies about 13–25 min after the pressure increase. As the strong P_{sw} compresses the dayside magnetosheath and, subsequently, the magnetotail, their magnetic fields intensify and activate stronger antiparallel reconnection on the dayside magnetopause first and near the central plasma sheet second. For southward IMF, dayside reconnection contributes to the CPCP enhancement 2–4 times more than nightside reconnection. For northward IMF, the dayside contribution weakens, and nightside reconnection contributes more to the CPCP enhancement. We find that high-latitude magnetopause reconnection during northward IMF produces sunward ionospheric plasma convection, which decreases the typical dawn-to-dusk ionosphere electric field. This results in a weaker dayside reconnection contribution to the CPCP during northward IMF.

1. Introduction

Recent studies have established that sudden enhancements of solar wind dynamic pressure (P_{sw}) result in intense magnetosphere-ionosphere interactions, indicating that P_{sw} enhancements can be a significant driver to transport solar wind energy into the magnetosphere-ionosphere (MI) system. The MI responses to strong solar wind pressure include auroral oval expansion [*Lyons et al.*, 2000; *Zesta et al.*, 2000; *Boudouridis et al.*, 2003, 2005], polar cap area reduction [*Boudouridis et al.*, 2003, 2004b, 2005], enhanced transpolar potential [*Boudouridis et al.*, 2004a, 2008b; *Ober et al.*, 2006, 2007], and fast ionospheric plasma convection [*Boudouridis et al.*, 2007, 2008a, 2011].

It has been inferred that during periods of strong solar wind pressure, magnetic reconnection intensifies in both the dayside and nightside magnetosphere. *Boudouridis et al.* [2007, 2011] analyzed the ionospheric convection patterns using Super Dual Auroral Radar Network (SuperDARN) observations and showed that the dayside ionospheric flow velocities in the vicinity of the expected dayside open-closed boundary (separatrix) location significantly increase within 4 min of the sudden enhancement of solar wind pressure, indicating strong magnetopause reconnection after the pressure impact. In addition, *Boudouridis et al.* [2011] observed a significant increase of the nightside ionospheric flow velocities 10–15 min after the P_{sw} impact, which implies intense nightside reconnection. Particle precipitation data from Defense Meteorological Satellite Program (DMSP) and auroral images from the Polar Ultra Violet Imager (UVI) [*Lyons et al.*, 2000; *Zesta et al.*, 2000; *Milan et al.*, 2004; *Hubert et al.*, 2006b, 2009; *Boudouridis et al.*, 2003, 2004b, 2008a] show that the

high-latitude auroral oval boundary moves poleward across the nightside region during strong solar wind pressure enhancements. This open flux reduction on the nightside magnetosphere is a direct indication of magnetotail reconnection enhancement.

Although previous studies have provided evidence of intensification of dayside and nightside reconnection, the following fundamental questions are still unanswered: (1) how the reconnection rates vary throughout the P_{sw} enhancement, (2) which physical process causes the reconnection rate increase, and (3) how strongly they contribute to the ionospheric convection enhancement that is simultaneously observed. Due to poor data coverage of satellite and ground observations throughout the entire MI system, these questions cannot be solved solely by observations. This paper addresses these open questions using the three-dimensional global magnetosphere-ionosphere-thermosphere model, Open Geospace General Circulation Model–Coupled Ionosphere Thermosphere Model (OpenGGCM-CTIM).

We simulate the magnetosphere-ionosphere responses to three P_{sw} enhancement events that occurred during negative, near-zero, and positive interplanetary magnetic field (IMF) B_z. *Zesta et al.* [2000] and *Boudouridis et al.* [2003, 2011] have investigated these events using ground magnetometer, DMSP, SuperDARN, and Polar UVI observations. We compare such observations with our model simulations of these events. The model-data comparison is conducted in a qualitative way to test whether the simulations follow general trends of the observations. Once we ascertain good agreement of our simulation results with key observations, we use the full 3-D global model results to investigate reconnection patterns in the dayside and nightside magnetosphere and quantify their relative importance to ionospheric convection. Our simulations compensate for the limited coverage of observations and provide insight into the physical cause of observed MI coupling effects.

In summary, we offer a physical insight, via model simulations, on when, where, and how solar wind energy is deposited into the magnetosphere-ionosphere system during the sudden enhancement of solar wind dynamic pressure. We introduce the detailed methodology in section 2 and conduct case studies of three P_{sw} enhancement events in section 3. Section 4 discusses reconnection patterns and their relation to the ionospheric convection. Finally, we summarize our results in section 5.

2. Methodology

2.1. OpenGGCM-CTIM Model

OpenGGCM-CTIM is a three-dimensional coupled magnetosphere-ionosphere-thermosphere model. It divides the Earth's geospace system into three regions—the magnetosphere, the MI coupling zone, and the ionosphere-thermosphere system—and applies different calculation strategies based on the main physical process of each region.

OpenGGCM calculates plasma behavior in the outer magnetosphere by solving resistive MHD equations as an initial-boundary-value problem. The inner boundary of the magnetosphere is located at 3–4 R_E from the center of the Earth, and its outer boundary extends to the OpenGGCM simulation box. The X range of the simulation box extends from 20–30 R_E sunward to 600–2000 R_E antisunward, and its Y/Z range is from -48 to +48 R_E. The simulation box is spacious enough to cover the whole magnetosphere and its surrounding environments such as bow shock and magnetosheath. In particular, the size of the simulation domain ensures supermagnetosonic velocities on all outer boundaries. This ensures that all flow characteristics are either inward (on the sunward side) or outward (on all other sides) so that the boundaries create no unwanted perturbations. The numerical grids are nonuniform Cartesian grids with small grid spacing (~0.1–0.2 R_E) near the dayside magnetosphere and near $Y_{gse} = Z_{gse} = 0$, where magnetic reconnection is expected to occur. OpenGGCM uses solar wind conditions from ACE, WIND, or Geotail spacecraft as input and provides number density, velocity, plasma pressure, and electromagnetic fields as output.

The MI coupling regime extends from the ionosphere to the inner boundary of the MHD calculation, at ~3.5 R_E from the Earth center. In this region, the MHD equations are not solved, but relevant quantities such as field aligned currents (FAC) and the electric potential are mapped back and forth between the magnetosphere and the ionosphere. Also, electron precipitation parameters are computed from magnetosphere parameters and mapped to the ionosphere, where they are used in CTIM. The OpenGGCM assumes a two-dimensional electrodynamic ionosphere and uses an ionospheric potential equation as a

function of Field Aligned Currents (FACs) and ionospheric conductance by assuming that the FACs generated from the solar wind–magnetosphere interaction should be closed in the ionosphere [*Raeder et al.*, 1998, 2001; *Raeder*, 2003]. To calculate the electric potential, OpenGGCM obtains FACs from the inner boundary of the magnetosphere and maps them to the ionosphere along the dipole magnetic field lines. Ionospheric conductance is obtained from CTIM, which is a three-dimensional dynamic model of the ionosphere-thermosphere system that self-consistently solves both neutral and ion fluid equations from 80 km to several 1000 km in altitude, providing realistic ionospheric conductance to OpenGGCM. Finally, the OpenGGCM maps the obtained electric potentials back to the inner boundary of the magnetosphere and uses them to provide the magnetospheric plasma flow boundary conditions on that boundary, closing the electrodynamic MI coupling cycle originally developed by *Vasyliunas* [1970] and *Wolf* [1975, 1983]. More detailed information about the OpenGGCM and CTIM models can be found in *Raeder et al.* [2001, 2008]; *Raeder* [2003] and *Fuller-Rowell et al.* [1996].

2.2. Calculation of Reconnection Rates

Under the assumption of a quasi-static magnetosphere, the dayside and nightside reconnection rates (Φ_D and Φ_N) are given by the integral of $E \cdot dl$ along the dayside and nightside open-closed field line boundary (OCB), where electric field $\boldsymbol{E}$ is $(V_b - V_p) \times B$ and dl is an infinitesimal distance along OCB. V_b and V_p are the normal velocity of the OCB and the velocity of the ionospheric plasma flow perpendicular to the OCB, respectively. Thus,

$$\Phi = \int (V_b - V_p) \times B \cdot dl$$

The term $V_b - V_p$ indicates the ionospheric flow in the OCB moving frame of reference. $E = (V_b - V_p) \times B$ is therefore the ionospheric electric field in the OCB moving frame of reference which should be equal to the electric field at the distant merging site assuming no field aligned potential drops and no inductive electric fields. If the OCB is stationary (i.e., $V_b = 0$), then the reconnection rate is equivalent to the electrostatic potential along the OCB. This calculation method is adopted from previous observational and theoretical studies on merging rates [*de La Beaujardiere et al.*, 1991; *Blanchard et al.*, 1996; *Ober et al.*, 2001, 2007; *Hubert et al.*, 2006a].

To obtain the open-closed field line boundary, we trace magnetic field lines from every ionospheric grid point through the magnetosphere. The ionosphere grid resolution is $3° \times 0.5°$ in magnetic longitude and latitude, respectively. We stop tracing when the field line returns to the inner boundary of the magnetosphere, when it reaches the outer boundary of the simulation box or when its length exceeds 1000 R_E. If a field line reaches the inner boundary, we consider it to be as a closed field line; otherwise, it is assumed to be an open field line. We mark the ionospheric grids connected to closed and open field lines with -1 and 1, respectively. The zero contour of those grids is the OCB. To determine the dayside and nightside open-closed field line boundary, we calculate ionospheric electric potentials along the OCB from the OpenGGCM-CTIM results and select the locations of maximum and minimum potentials which appear at the dawn and dusk sectors, respectively. The dayside OCB is the region from maximum to minimum potentials that crosses the dayside ionosphere, and the nightside OCB is the remainder.

In order to obtain the dayside reconnection rate, we calculate the first term of the reconnection rate integral, $\int V_b \times B \cdot dl$, by measuring the open flux per unit time crossing the dayside open closed field line boundary and the second term, $-\int V_b \times B \cdot dl$, by obtaining the electric potential difference along the dayside OCB. The same procedure is applied for the calculation of nightside reconnection rate except that the two nightside integrals are measured along the nightside OCB.

Note that we assume no potential drop along the magnetic field lines. Under this assumption, the electric potential across magnetospheric reconnection lines is projected to the ionosphere. However, the numerical model solves the MHD equations on a grid, such that the discretization may introduce nonphysical parallel electric fields along the field lines. Due to this numerical artifact, the reconnection rates calculated from ionospheric variables may not exactly match the reconnection rates in the magnetosphere. The numerically induced potential drop ranges a few kilovolts to ~10 kV in the model, while the reconnection rate varies from several tens to hundreds of kilovolts. Thus, the potential drop between the reconnection line and the

ionosphere is minimal, compared to the reconnection rate, and therefore, any mismatch between the magnetospheric and ionospheric electric potentials can be neglected for the purpose of this study.

2.3. The Relation Between Reconnection Rates and CPCP

This paper investigates the balance of dayside and nightside reconnection rates and their relative contribution to a dramatic increase of ionospheric flows that occurs immediately following a sharp magnetospheric compression. To explain such a relation, we adopt the cross polar cap potential (CPCP) as a proxy of the ionospheric convection strength, and fit our model results to the CPCP equation of the expanding and contracting polar cap (ECPC) model [*Lockwood*, 1991; *Lockwood and Cowley,* 1992]:

$$\Phi_{\mathrm{CPCP}} = C_D\Phi_D + C_N\Phi_N + \Phi_V$$

where Φ_{CPCP} is a transpolar potential, Φ_V is the viscous-like potential, and Φ_D (Φ_N) is the electric voltage caused by dayside (nightside) reconnection. C_D and C_N are regression coefficients of the dayside and nightside merging rate, respectively. These coefficients have been considered as weight factors that quantify the relative contribution of merging rates on the CPCP enhancement [*Lockwood et al.*, 2009; *Gordeev et al.*, 2011]. Note that in steady state, when the dayside and nightside OCB motion is zero, $\Phi_D = \Phi_N = \Phi_{CPCP} - \Phi_V$ and then the regression coefficients are $C_D = C_N = 0.5$. Therefore, any difference of the coefficients from 0.5 could be interpreted to indicate departures from steady state and then they would also represent the relative contributions of the two reconnection rates to the CPCP.

This paper defines the CPCP to be the difference between the maximum and minimum ionospheric potentials. CPCP is produced by the combined effect of reconnection and viscous interaction. Assuming that the potential difference along the OCB (ΔP_{OCB}) is driven by magnetic reconnection, the viscous-like potential (Φ_V) becomes $\Phi_v = CPCP - \Delta P_{\mathrm{OCB}}$. We use a multiple linear regression to fit our model results of reconnection rates and viscous potential to the above CPCP equation, and obtain the regression coefficients that give the best fit results.

3. Case Studies

3.1. Event 1: 10 January 1997

The first event occurred during the recovery phase of a geomagnetic storm on 10 January 1997. Figures 1a–1d show IMF, solar wind speed, number density, and dynamic pressure obtained from the OMNI data during this event. The solar wind pressure increases from 2 to 6 nPa for 20 min, while IMF stays southward. The vertical thick black line represents the arrival of a strong pressure front at the nose of the magnetopause. Previous studies of this event [*Lyons et al.*, 2000; *Zesta et al.*, 2000; *Boudouridis et al.*, 2003, 2005] have shown auroral oval expansion, polar cap closure, and enhanced CPCP.

The OpenGGCM-CTIM model simulates the magnetosphere-ionosphere responses to this event using solar wind parameters as input. Figure 1e shows the polar cap area obtained from our model. After a few minutes of slight expansion near 11:00 UT, the modeled polar cap area continuously shrinks until 11:27 UT. Polar UVI Imager [*Zesta et al.*, 2000] and DMSP SSJ/4 instruments [*Boudouridis et al.*, 2003] also observe the polar cap closure after the pressure impact, agreeing with our model results.

Figure 1f displays the cross polar cap potentials obtained by OpenGGCM-CTIM (blue line), assimilative mapping of ionospheric electrodynamics (AMIE) technique (green line) and DMSP spacecraft (red dots). The red horizontal lines represent the time periods for the spacecraft to estimate each CPCP value. DMSP satellites obtain a transpolar potential by integrating measured electric fields along the satellite trajectory that crosses the entire polar region. Thus, they provide an averaged picture of the CPCP and may miscalculate its magnitude if the DMSP orbit misses the center of the ionospheric potential pattern.

To compensate for this limitation, we use AMIE predictions of transpolar potential as additional data source for model-data comparison. The AMIE technique estimates the entire ionospheric electrodynamics, such as electric potentials, conductances, and currents, by assimilating the observations from radar, ground magnetometer, and low-orbiting satellites. During intervals of good data coverage, AMIE provides reasonable electric field maps with an uncertainty of ~30% [*Knipp and Emery*, 1997]. The AMIE data presented in this paper are calculated from 115–135 ground magnetometers and downloaded from http://vmr.engin.umich.edu/Model/_amie/.

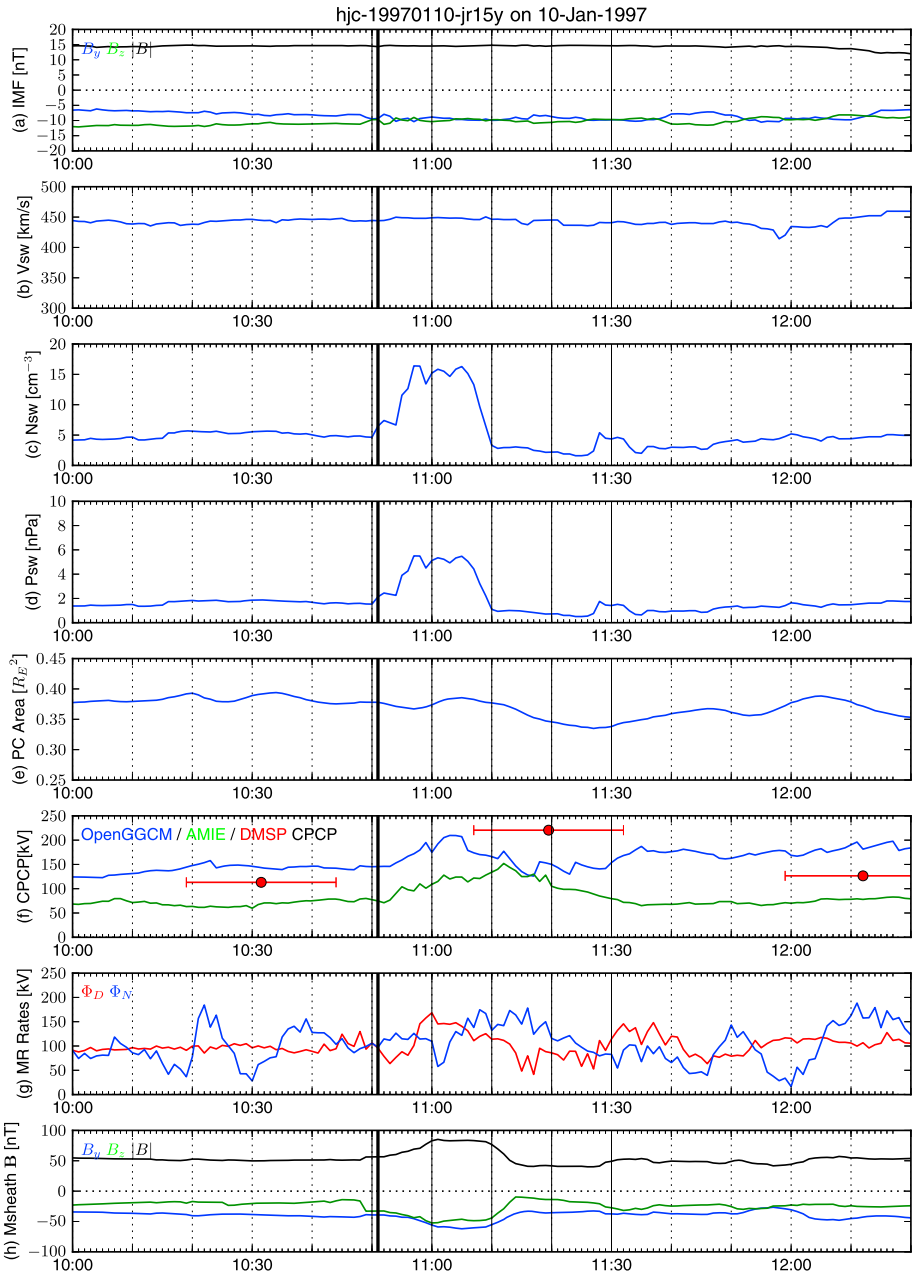

Figure 1. (a–d) The OMNI solar wind data and (e–h) the OpenGGCM-CTIM results on 10 January 1997. IMF, solar wind plasma speed (V_{sw}), number density (N_{sw}), and dynamic pressure (P_{sw}) as shown in Figures 1a–1d. The polar cap area, cross polar cap potential, reconnection rates, and magnetosheath magnetic fields obtained from the OpenGGCM-CTIM model are shown in Figures 1e–1h. The red dots and horizontal lines in Figure 1f represent DMSP transpolar potentials and the observation periods for the satellites to measure each CPCP. The blue and green lines in Figure 1f show the cross polar cap potentials predicted from OpenGGCM-CTIM and AMIE. The red and blue lines in Figure 1g are the reconnection rates of dayside and nightside magnetosphere, respectively. The thick vertical lines indicate when the P_{sw} enhancement arrives at the nose of the magnetopause, and the thin vertical lines represent the times selected for the magnetosphere plots. All magnetic field vectors are in the GSE coordinate system.

We use both the DMSP and AMIE data to understand the general trend of CPCP and to test our model results. In Figure 1f, DMSP data show CPCP enhancement from 120 to 220 kV after the pressure impact, while AMIE shows a similar CPCP response although its magnitude is lower than the DMSP data. Our model also shows a CPCP increase from 140 to 200 kV after the pressure change. Although the CPCP magnitudes are

different, all the DMSP, AMIE, and OpenGGCM-CTIM data consistently and clearly show the enhancement of the transpolar potential after the pressure impact.

Differences of CPCP values from different data sources have been noticed in the previous studies. *Kihn et al.* [2006] showed that AMIE produces higher transpolar potentials than DMSP spacecraft if ground magnetometer data are used as the only input for AMIE. *Slinker et al.* [1999] and *Raeder* [2005] found that MHD models tend to predict higher CPCP than AMIE. In spite of the difference in CPCP magnitude, these studies showed a reasonable correlation between the DMSP and AMIE data and between the AMIE and MHD data, supporting that our qualitative model-data comparison with these CPCP data are reliable.

Figure 1g shows the reconnection rates of OpenGGCM-CTIM. These rates are calculated based on the method presented in section 2.2. The dayside reconnection rate (Φ_D) reacts first to the P_{sw} enhancement, increasing from 60 to 160 kV within a few minutes after the pressure change. The polar cap expands near ~11:00 UT due to the enhanced dayside reconnection rate (see Figure 1e). The nightside reconnection rate (Φ_N) reaches its maximum value at 11:09 UT, ~9 min later than the dayside reconnection rate does. The magnetotail reconnection becomes stronger than the magnetopause reconnection during 11:05–11:27 UT. As a result, the polar cap area decreases continuously until the next, relatively weak pressure enhancement hits the dayside magnetosphere at 11:27 UT.

To understand why magnetopause reconnection intensifies during a P_{sw} enhancement, we display magnetic fields of the magnetosheath in Figure 1h, which are obtained from the model results at 1 R_E sunward from the magnetopause nose. Although the IMF magnitude is steady during that time (black line in Figure 1a), the total magnetic field of the magnetosheath (black line in Figure 1h) jumps up to 85 nT in response to the solar wind pressure increase. The total magnetosheath field drops quickly as the P_{sw} decreases at ~11:07 UT and enhances again as the P_{sw} slightly increases at 11:27 UT, so it varies in phase with P_{sw}. Thus, the sudden increase of solar wind dynamic pressure compresses the magnetosheath total magnetic field, which in turn increases the reconnection rate. This increase is analogous to the well-known pileup reconnection first discussed by *Parker* [1973] and *Sonnerup* [1988]. As a result, stronger magnetosheath fields drape over the dayside magnetopause, activating more intense antiparallel reconnection and thus increasing the dayside merging rate [see *Dorelli et al.*, 2004].

Figure 2 displays the magnetosphere noon-midnight meridian plane during this event and examines the dynamics of different variables. The dynamic pressure (P_{dy}), X component of velocity (V_x) in geocentric solar ecliptic (GSE) coordinate system, total magnetic field ($|B|$), and X component of the magnetic field (B_x) in GSE coordinate system are plotted from left to right. We display the model output with a time resolution of 10 min from 10:50 to 11:30 UT as demonstrated from top to bottom of each column in Figure 2. The thin vertical lines in Figure 1 correspond to the timing of each column of Figure 2.

Figures 2a and 2b show the magnetosheath compression due to the sudden enhancement of the solar wind dynamic pressure. The nose of the bow shock moves from $X_{gse} = 17$ to 11 R_E at 11:00 UT. This compression intensifies the total magnetic field of the magnetosheath and strengthens magnetopause reconnection. Figures 2c and 2d show the magnetosphere state when the solar wind pressure decreases to ~1 nPa, after the first compression, and when the bow shock location moves out to $X_{gse} = 24$ R_E at 11:20 UT. Because of the magnetosheath expansion, both the total magnetosheath field and dayside merging rate weaken at that time. The magnetosheath is compressed again at 11:30 UT when the smaller pressure enhancement arrives at the dayside magnetopause (see Figure 2e). The bow shock moves back to $X_{gse} = 22$ R_E, which leads to the slight increase of the magnetosheath fields and of the dayside merging rate.

Figures 2c–2e show that the sudden increase of solar wind pressure also affects the nightside magnetosphere. The pressure front reaches the near-Earth magnetotail (X_{gse} from -20 to -40 R_E) at 11:10 UT and propagates to the distant tail ($X_{gse} < -80$ R_E) at 11:20 and 11:30 UT. As the pressure compresses the magnetotail, the magnetic field B_x near the central plasma sheet increases in both lobes. This leads to a stronger antiparallel reconnection near $X_{gse} = -30$ R_E with faster earthward flows, as evidenced in the V_x panel. At 11:30 UT, the P_{sw} enhancement disappears to the very distant magnetotail. As a result, the near-Earth magnetotail expands and its magnetic field decreases. The earthward plasma speed also reduces to ~200 km/s, as a result of weaker nightside reconnection.

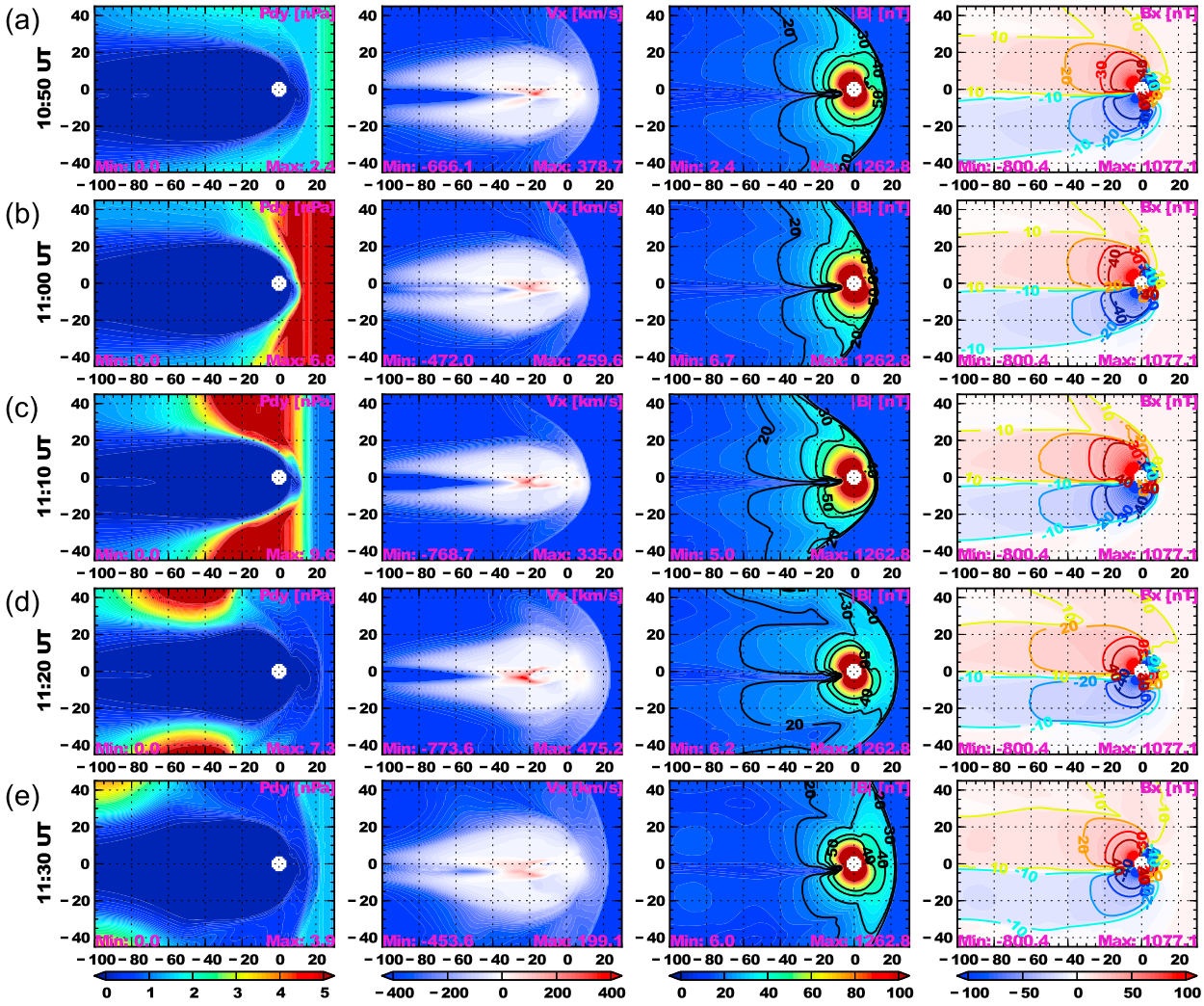

Figure 2. (a–e) The OpenGGCM-CTIM magnetosphere plots during 10:50–11:30 UT on 10 January 1997. Each column represents from left to right the dynamic pressure (P_{dy}), X_{gse} component of plasma velocity (V_x), total magnetic field ($|B|$), and X_{gse} component of magnetic field (B_x) on the noon-midnight meridian plane.

The compression by the P_{sw} enhancement intensifies magnetic fields of the magnetosheath and near the central plasma sheet, increasing dayside and nightside reconnection rates, respectively. Based on Figures 2b and 2c, the P_{sw} front takes about 10 min to move from the dayside to the nightside magnetosphere. This explains why the nightside reconnection responds to the pressure impact ~9 min later than the dayside reconnection. The polar cap area thus expands for a short time period after the pressure impact due to the enhancement of dayside merging rate, but it soon closes when the nightside reconnection rate becomes dominant.

3.2. Event 2: 30 April 1998

The second event occurred on 30 April 1998 during nearly zero IMF B_y and B_z. Figures 3a–3d show IMF (in GSE coordinates), solar wind plasma speed, number density, and dynamic pressure observed by the WIND spacecraft. The solar wind data are time-shifted to account for the solar wind propagation from the WIND location to the nose of the magnetopause. At 09:25 UT, a shock impacted the magnetosphere. Solar wind number density and velocity abruptly increased, intensifying the solar wind dynamic pressure from 2 to 12 nPa. The IMF points southwest for the first 2 h of the P_{sw} enhancement and turns northeast after 11:30 UT. The major difference between this event and the previous one is that P_{sw} remains increased for several hours during relatively weak IMF conditions, so it is a step change rather than a pulse.

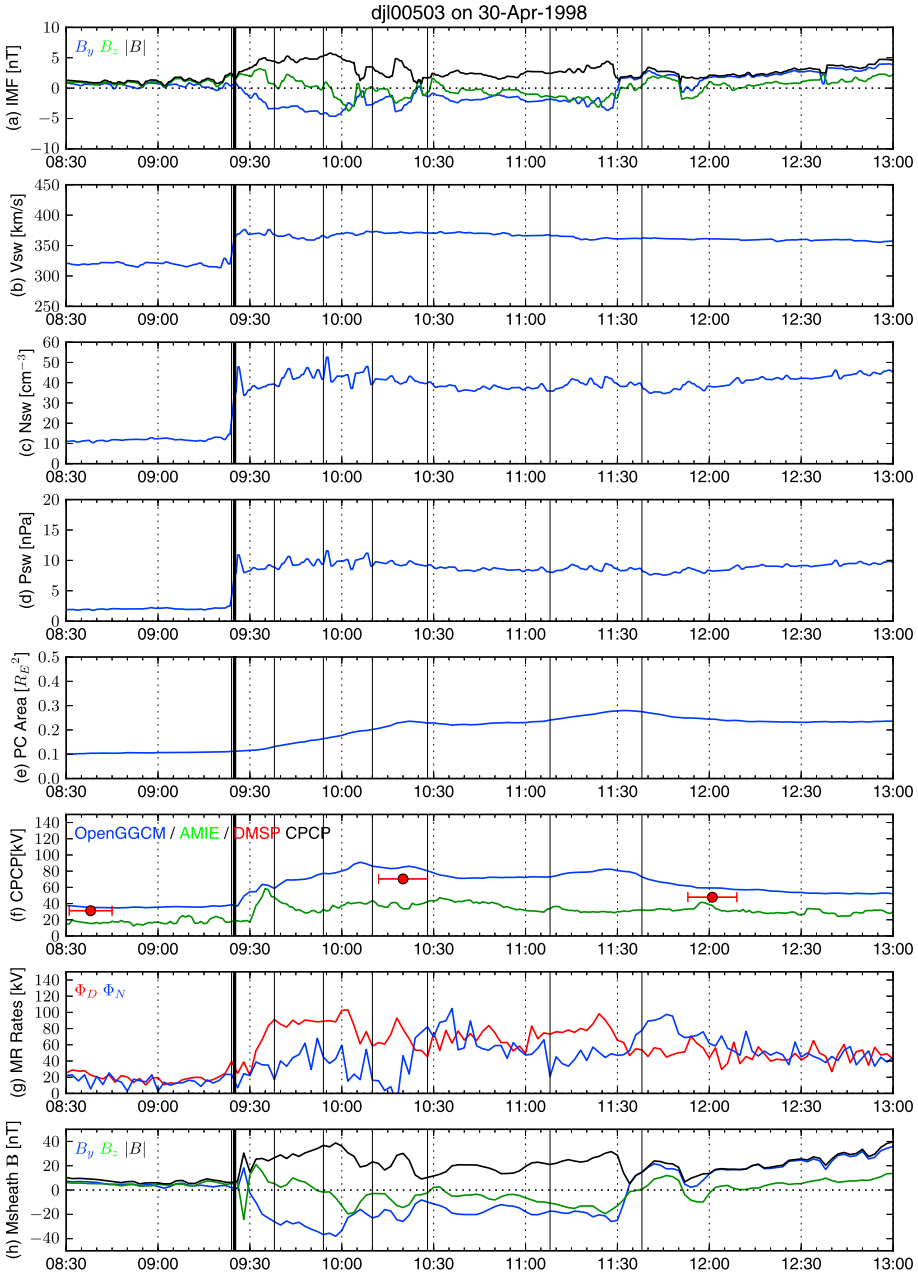

Figure 3. (a–d) The WIND spacecraft measurements of solar wind conditions and (e–h) the OpenGGCM-CTIM results on 30 April 1998. The WIND data are time shifted to account for the solar wind propagation from the satellite location to the magnetopause nose. See descriptions of Figure 1 for more details.

Figures 3e–3h show the polar cap area (area of open flux), transpolar potential, dayside and nightside reconnection rates, and magnetosheath fields calculated from our simulation of this event in the same format as in Figure 1. The blue line, green line, and red dots in Figure 3f represent the time series of the CPCP calculated by our simulation, AMIE, and DMSP observations, respectively. Similarly, the red horizontal lines in Figure 3f represent the amount of time a full crossing of the auroral oval is completed by a DMSP satellite in order for a single value of CPCP to be calculated. As we noted above, each single CPCP value represents an average of the transpolar potential for the time period indicated by the red lines.

The modeled polar cap expands continuously during the first 2 h of P_{sw} enhancement (Figure 3e). Most of this time, IMF is weakly southward (−2 to −3 nT in the solar wind and −10 to −20 nT in the magnetosheath).

The total magnetosheath field intensifies when the shock arrives, as expected. As a result, dayside reconnection significantly increases and the polar cap area opens. At 11:30 UT, the magnetosheath field turns northward. Dayside reconnection weakens, and nightside reconnection plays a dominant role in the MI system, which leads to a polar cap closure.

Reduction of open flux area and polar cap size after the solar wind pressure enhancements has been observed in several studies [*Zesta et al.*, 2000; *Boudouridis et al.*, 2003, 2004b, 2005; *Hubert et al.*, 2006b, 2009; *Milan et al.*, 2009]. Depending on the IMF conditions, the closing happens only on the nightside and flank regions or over the whole magnetic local time (MLT) locations including the dayside area [*Boudouridis et al.,* 2003, 2004b]. For this event, *Boudouridis et al.* [2004b] measured the poleward boundaries of auroral precipitation from a total of 16 DMSP satellite crossings over the pole region and estimated the polar cap boundary motion after the P_{sw} impact. Due to the poor data coverage on the dayside ionosphere, they could not identify the dayside boundary motion, but observed that the nightside polar cap boundary moves poleward after the P_{sw} enhancement. This indicates closing of the nightside polar cap.

The polar cap area is not a straightforward metric for the purpose of model-data comparison, due to the lack of complete MLT coverage of observations at the OCB and the nonsmooth OCB produced by the model simulations. *Boudouridis et al.* [2004b], for this same event, estimated the poleward boundary based on only a few data points observed at different times between 09:40 and 11:25 UT. Our model produces very complicated polar cap boundaries during this observation period. Although the one-to-one comparison is difficult, our model shows an increase of the nightside reconnection rate during 9:25–9:50 UT and 10:20–10:45 UT (see Figure 3g). This indicates that the polar cap closes, at least on the nightside, twice in our model during the DMSP observation time. Hence, while our model indicates overall opening of the polar cap area, it does capture correctly some of the observational elements, and more than likely the balance between dayside and nightside reconnection rates may be different in the simulation environment than in the actual observations.

Unlike the motion of polar cap boundary, the CPCP shows excellent agreement between the model output and DMSP observations (see a blue line and red dots in Figure 3f), demonstrating that our simulation provides a realistic response of ionospheric convection. The modeled CPCP increases to ~90 kV at 10:05 UT, after the compression, and then slowly decreases to ~50 kV for the next several hours, even though the solar wind dynamic pressure remains at high levels. DMSP observations show similar CPCP increase from 35 to 70 kV at 10:20 UT, and its subsequent decrease to 50 kV at 12:00 UT. Although predicting lower CPCP values than DMSP, AMIE produces a qualitatively similar CPCP response and confirms that the DMSP transpolar potentials are reliable.

Figure 3g shows the reconnection rates of OpenGGCM-CTIM. The dayside reconnection rate increases from 20 to 90 kV within 10 min after the P_{sw} increase. After this sudden rise, the rate slowly decreases for the next 3 h. Unlike the first event, this is a shock, so the sharp solar wind dynamic pressure jump is accompanied by a similar increase in the IMF magnitude. Both of those contribute to a significant magnetopause reconnection increase, although we are not able to identify which parameter (P_{sw} or IMF) contributes more to the enhancement of dayside reconnection.

The nightside merging rate shows a more complex response than in our previous event. After the pressure impact, it exhibits three consecutive enhancements with local maximum at 09:50, 10:40, and 11:45 UT, the first peak occurring ~15 min after the dayside reconnection peak. To understand the nightside dynamics, snapshots of the modeled magnetosphere at 09:24, 09:38, 09:54, 10:10, 10:28, 11:08, and 11:38 UT are displayed in Figures 4a–4g. The timing of each snapshot is also shown as a thin vertical line in Figure 3. Each column of Figure 4 represents, from left to right, the dynamic pressure ($P_{dy} = \rho v^2$), plasma pressure ($P_p = nkT$), X_{gse} component of plasma velocity (V_x), and X_{gse} component of magnetic field (B_x) on the noon-midnight meridian plane.

Figures 4a–4c show the magnetosphere before and right after the pressure impact. At 09:24 UT, the pressure front has not yet reached the dayside magnetopause. Our model observes magnetotail reconnection near $X_{gse} = -18\ R_E$ evidenced by the oppositely directed fast plasma flows there. At 09:38 UT, the pressure front moves to the near-Earth magnetotail. The fast earthward flow of the prior instance significantly reduces now, indicating that the previous nightside reconnection subsides. As the P_{sw} compresses the magnetotail

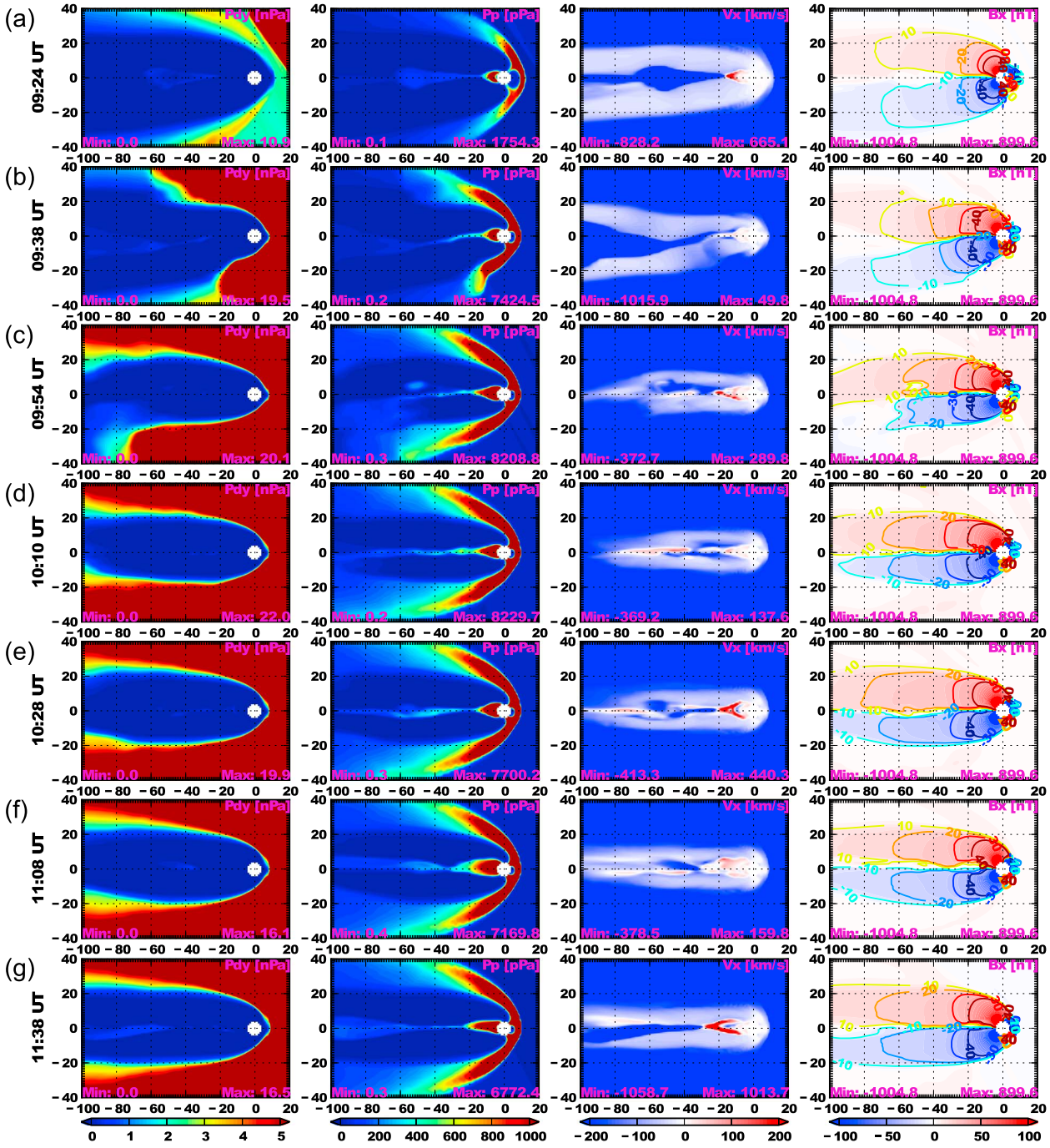

Figure 4. (a–g) The OpenGGCM-CTIM magnetosphere plots during 09:24–11:38 UT on 30 April 1998. Each column displays from left to right the dynamic pressure (P_{dy}), plasma pressure (P_p), X_{gse} component of plasma velocity (V_x), and X_{gse} component of magnetic fields (B_x) on the noon-midnight meridian plane. The times of each magnetosphere plot are marked as thin vertical lines in Figure 3.

at09:38 UT, the central plasma sheet stretches out into the more distant tail, as evidenced by the intensification of plasma pressure along the X axis in Figure 4b. At the same time, the magnetic field B_x increases in both the northern and southern magnetotail lobes. At 09:54 UT, the pressure front has reached the distant tail; thus, a broader region of the nightside magnetosphere is being compressed and B_x near the central plasma sheet continues to increase. This initiates antiparallel reconnection near $X_{gse} = -27\ R_E$, creating again fast earthward plasma flows.

Figures 4d–4g show the magnetosphere after the strong pressure has engulfed most of the magnetotail. At these times, the impact of solar wind pressure front disappears and the nightside magnetosphere adjusts to the new high pressure level. The dayside merging rate stays high until 11:30 UT and loads solar wind field and plasma in the magnetotail lobes. As a result, our model observes a plasmoid structure near $X_{gse} = -25\ R_E$ at 10:10 UT and a thick and dense plasma sheet at 11:08 UT (see the plasma pressure in the third columns of Figures 4d and 4f). When the magnetosheath field turns northward at the instances of 10:28 and 11:35 UT, the nightside reconnection dominates and sends the previously piled up plasma back to the inner magnetosphere with strong earthward flows at 10:28 and 11:39 UT.

The magnetotail compression by the P_{sw} enhancement produces the first peak of the nightside reconnection rate at 09:50 UT. As the pressure maintains its strength for several hours, the magnetotail adjusts to the new pressure strength, repeating the loading-unloading process. This creates the other nightside reconnection peaks at 10:28 and 11:35 UT, in Figure 3g.

3.3. Event 3: 12 October 2000

The last event is a shock that occurred on 12 October 2000 during northward IMF. Figures 5a–5d show the solar wind conditions observed by the Geotail spacecraft. At 22:29 UT, the solar wind pressure jumps from 1 to 6 nPa while the IMF magnitude increases from 5 to 15 nT. The enhanced P_{sw} and IMF are sustained for the next several hours, while the IMF B_z remains primarily northward with a strong positive B_y.

Figures 5e–5h show the OpenGGCM-CTIM results. Due to the enhancements of solar wind pressure and IMF magnitude, the total magnetosheath field intensifies. This leads to the increase of dayside reconnection rate and the opening of the polar cap area at ~22:37 UT. The nightside reconnection rate shows two local peaks at 22:42 and 23:11 UT. As this rate exceeds the dayside reconnection rate starting at ~22:45 UT, the polar cap area continuously shrinks. When the magnetosheath field turns slightly southward at 23:30 UT, the dayside reconnection abruptly increases and the polar cap area reopens, as seen in Figure 5e.

Figure 5f shows the transpolar potentials obtained from the OpenGGCM-CTIM (blue line), AMIE (green line), and DMSP (red dots for the three available DMSP passes). The modeled CPCP jumps from 36 to 70 kV within a few minutes after the shock impact and slowly increases for the remainder of this period. The DMSP spacecraft do not observe the CPCP increase during the pass centered at 23:02 UT because that orbit does not cross high-latitude ionosphere (the highest latitude of this orbit is 75.87° magnetic latitude, while others are at least over 79.84° magnetic latitude), thus missing the potential pattern peaks and severely underestimating the CPCP. Over the following orbit centered at 23:50 UT however, DMSP does record a significant increase in the CPCP, as that orbit crosses near the center of the potential pattern (the orbit reaches up to 79.84° magnetic latitude). Due to the poor DMSP data immediately after the compression, we focus on the AMIE data instead for a model-data comparison. Both AMIE and OpenGGCM-CTIM observe significant CPCP enhancement up to 70 kV at 22:32 UT, the increase lasting for many hours after the initial compression as the P_{sw} remains at high levels as well.

The reconnection patterns in Figure 5g are also consistent with the responses of the ionospheric plasma flows. This event has been studied before by *Boudouridis et al.* [2011], who used the SuperDARN observations to show a dramatic enhancement of the dayside ionospheric flows at ~22:35 UT, immediately after the compression. The reconnection patterns that we calculated and which are shown in Figure 5g are consistent with the *Boudouridis et al.* [2011] observations. The dayside merging rate from our simulation in Figure 5g increases at ~22:37 UT, just when *Boudouridis et al.* [2011] observed the dayside flow enhancement. The nightside reconnection rate from our simulation reaches its first peak at 22:42 UT and increases significantly around 23:10 UT in Figure 5g. This is also in complete agreement with the *Boudouridis et al.* [2011] results, which observed the first enhancement of nightside flows at ~22:42 UT, and the spreading of the fast flow to a much broader region of the nightside ionosphere during 22:54–23:16 UT.

The dayside merging rate increases as the total magnetosheath field intensifies due to the combined effect of P_{sw} and IMF enhancements. Therefore, for this event, the dayside reconnection increase is not solely due to the P_{sw} enhancement. The nightside merging rate enhances as the strong solar wind pressure compresses the magnetotail. Figure 6 shows this compression process. It displays the noon-midnight meridian of key magnetospheric properties in a similar format as Figure 4. The five rows are single instances from 22:30 to

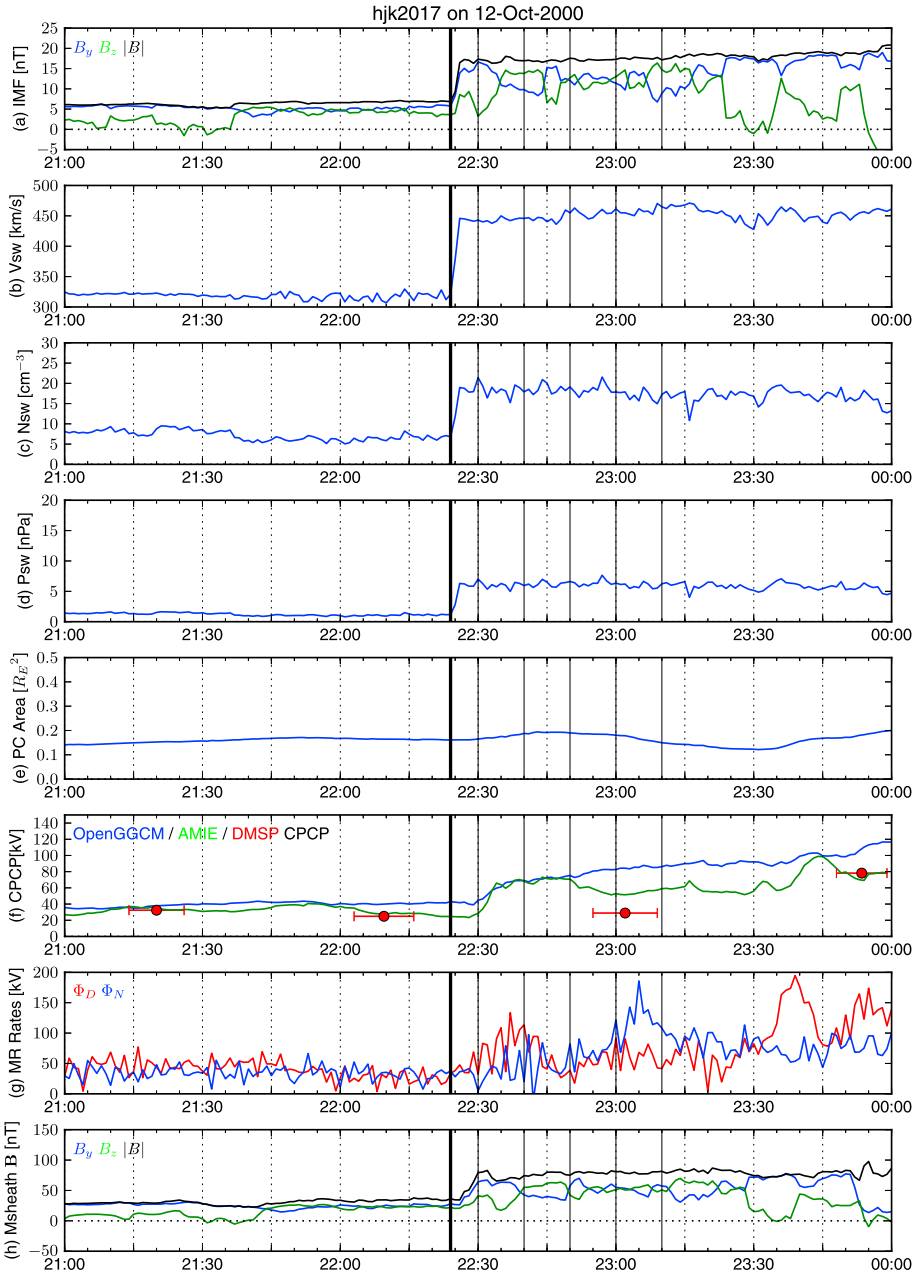

Figure 5. (a–d) The Geotail spacecraft measurements of solar wind conditions and (e–h) the OpenGGCM-CTIM model results on 12 October 2000. See descriptions of Figure 1 for more details.

23:10 UT, 10 min apart. The dynamic pressure (P_{dy}), X_{gse} component of plasma velocity (V_x), and X_{gse} component of magnetic field (B_x) are plotted in columns from left to right.

Figures 6a and 6b show the magnetosphere before and after the P_{sw} enhancement. At 22:30 UT before the pressure impact, the nightside magnetosphere is quiet without fast plasma flows. As the strong pressure compresses the near-Earth magnetotail at 22:40 UT, the magnetic field B_x increases in opposite directions near the central plasma sheet, initiating antiparallel reconnection near $X_{gse} = -30\ R_E$ with fast earthward plasma flows. Figures 6c–6e show compression of the distant magnetotail. At 22:50 and 23:00 UT, the velocity of the earthward plasma flows reduces slightly from 630 km/s to ~500 km/s and gets more distributed along the length of the tail, indicating nightside reconnection activity occurring along a significant region of the tail between −30 and −80 R_E. The pressure front continues propagating downtail to

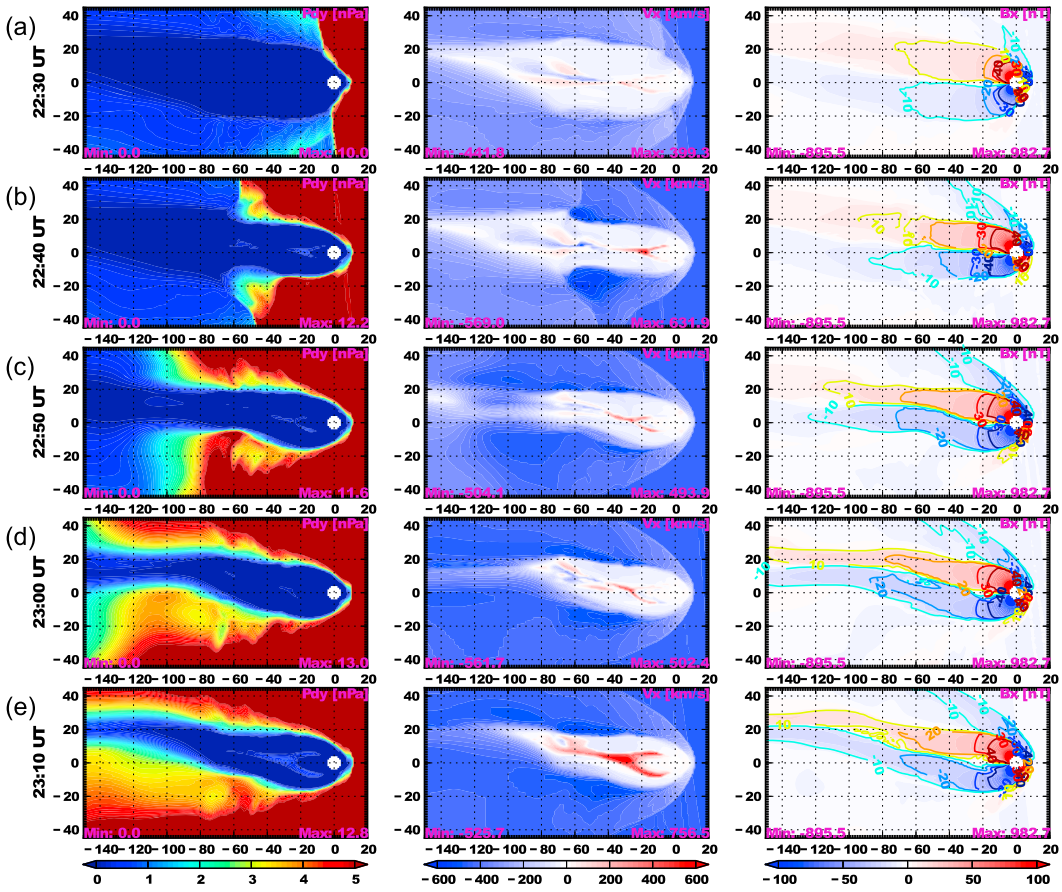

Figure 6. (a–e) The OpenGGCM-CTIM magnetosphere plots during 22:30–23:10 UT on 12 October 2000. Each column shows from left to right the dynamic pressure (P_{dy}), X_{gse} component of plasma velocity (V_x), and X_{gse} component of magnetic fields (B_x) on the noon-midnight meridian plane. The times of each magnetosphere plot are marked as thin vertical black lines in Figure 5.

a further distant tail region, compressing the whole length of the magnetotail. As a result, the magnetic field B_x increases from the near-Earth region to the very distant magnetotail, generating intense magnetic reconnection at 23:10 UT, evidenced by the strong Earthward flows in that instance. Thus, the P_{sw} enhancement of this event compresses the magnetotail strong enough to create two peaks of the nightside reconnection rate.

4. Discussion and Conclusion

4.1. The Reconnection Patterns During the Sudden P_{sw} Enhancement

Reconnection rates are difficult to estimate solely with observation because to calculate the merging rates, one needs to know the motion of open-closed field line boundary across all MLT and the electric field potential patterns over the entire ionosphere. Previous studies of the merging rates [*Blanchard et al.*, 1996, 1997; *Østgaard et al.*, 2005; *Hubert et al.*, 2006a] have estimated the OCB motions from 6300 Å auroral emission measurements and IMAGE FUV images, and the ionosphere electric potentials from Sondrestrom, EISCAT, and SuperDARN radar measurements. However, ground and space observations do not provide a complete coverage of the ionosphere, and therefore, the global merging patterns are difficult to obtain on a single case basis (only empirical patterns can be reliably assembled). Under such conditions, three-dimensional global magnetosphere-ionosphere-thermosphere modeling can complement the observations.

We simulated three events of sudden P_{sw} enhancements using OpenGGCM-CTIM and compared the results with DMSP, AMIE, and SuperDARN measurements. Our model produces to a reasonable extent the observed magnetosphere-ionosphere responses, especially the transpolar potential enhancement. The

modeled CPCP shows generally good agreement with the DMSP observations and AMIE predictions. We now focus on these successful simulation results to investigate the reconnection patterns during strong solar wind dynamic pressure within the value space of the simulation box.

Our model results show that the dayside reconnection rate increases ~2 min after the P_{sw} enhancements and reaches its maximum within 9–12 min after the P_{sw} impact. Note that our reconnection rate is calculated based on the ionospheric values. Considering that a typical Alfven wave transit time between the magnetosphere and the ionosphere is ~2 min, reconnection at the dayside magnetopause intensifies immediately following the arrival of P_{sw} enhancements. The nightside reconnection rate reacts later than the dayside rate and takes 13–25 min to reach its maximum after the pressure change. The response time scales generally match the timing of observed ionospheric convection enhancements. The SuperDARN radar observations [*Boudouridis et al.*, 2011] have shown a dramatic increase of dayside ionospheric flows within 10 min of pressure impact and nightside flow enhancements in 15–20 min after the impact, in agreement with our results of the response of the dayside and nightside reconnection rates.

The dayside reconnection rate increases due to magnetosheath compression during strong solar wind pressure. This compression strengthens magnetic fields in the magnetosheath, intensifying antiparallel reconnection on the dayside magnetopause, as predicted by theoretical merging models [*Parker*, 1973; *Sonnerup*, 1988; *Dorelli et al.*, 2004]. The first event on 10 January 1997 clearly shows this process. However, in the last two events on 30 April 1998 and 12 October 2000, it is difficult to isolate this effect because the solar wind pressure enhancements are accompanied by an increase of total IMF magnitude, which in itself will have the same effect on dayside reconnection rate.

The nightside reconnection rate intensifies when strong solar wind pressure compresses the magnetotail. The B_x intensifies in the northern and southern lobes due to this compression, intensifying antiparallel reconnection near the central plasma sheet. All three event studies show the enhancement of nightside reconnection rate due to the magnetotail compression. After the compression front moves into the distant magnetotail, the nightside magnetosphere behaves differently at each case, depending on whether the whole magnetosphere remains engulfed in the region of high pressure (step increase) or not (pulse increase) and on the concurrent IMF orientation.

On 10 Janaury 1997, the compression is a pulse and P_{sw} decreases after the initial increase to almost preincrease levels, followed shortly afterward by a smaller increase. The magnetotail experiences both of these successive compressions, and the nightside reconnection rate increases after each compression and proportionally to the strength of each compression, all of that occurring under strong southward IMF. On 30 April 1998, the compression is a step increase with the pressure remaining at high levels for many hours under very weak southward or near-zero IMF. Under such conditions, the nightside magnetosphere repeats the loading-unloading process as the enhanced dayside reconnection continuously loads the solar wind plasma into the magnetotail lobes. On 12 October 2000, the P_{sw} enhancement is also a step increase lasting for many hours under northward IMF. In this case, the whole magnetotail gets compressed down to the more distant magnetotail, dramatically increasing the nightside reconnection rate.

4.2. The Relation Between the Reconnection Rates and the Transpolar Potential

To understand the relative importance of dayside and nightside reconnection on the CPCP enhancement, we use the previously defined CPCP function of the expanding and contracting polar cap (ECPC) model. This model introduces CPCP (Φ_{CPCP}) as a function of dayside and nightside reconnection rates (Φ_D and Φ_N) by assuming that the electric voltages across the dayside and nightside reconnection lines are distributed along the open-closed field line boundaries [*Lockwood*, 1991]. Later, the model added the viscosity effect (Φ_V) to get equation $\Phi_{CPCP} = C_D\Phi_D + C_N\Phi_N + \Phi_V$ where C_D and C_N are regression coefficients of the dayside and nightside reconnection rates, respectively [*Lockwood and Cowley*, 1992]. The regression coefficients can be considered to be a weighting factor that quantifies the contribution of each merging rate on the transpolar potential [*Lockwood et al.*, 2009; *Gordeev et al.*, 2011]. Here, we apply a multiple linear regression method to estimate the regression coefficients and determine which reconnection dominates the CPCP, based on the above equation.

One may question whether the regression coefficients explain a cause-effect relationship between reconnection and CPCP because if an equation is given, the multiple linear regression method only provides

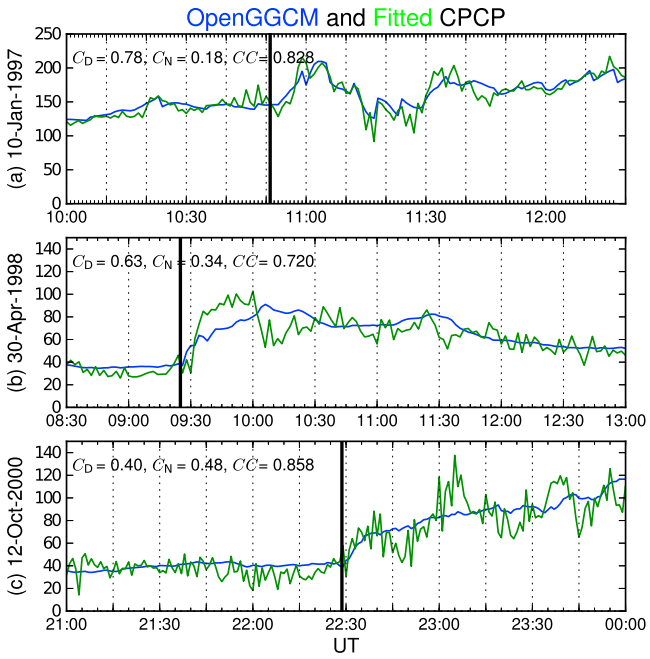

Figure 7. The CPCP fitting results of all three events. The blue and green lines are the transpolar potentials obtained from the OpenGGCM-CTIM and the multiple linear regression analysis, respectively. The upper right corner of each panel displays the regression coefficients (C_d and C_n) and the correlation coefficient (CC) between the modeled and fitted CPCPs.

correlation between any parameters regardless of their actual physical relationship. However, dayside and nightside reconnection rates have been described as CPCP contributors in previous publications [for example, *Reiff et al.*, 1981; *Boyle et al.*, 1997; *Bristow et al.*, 2004; *Milan*, 2004; *Milan et al.*, 2007; *Lockwood et al.*, 2009]. Several experiments using the ECPC model [*Milan*, 2004; *Lockwood et al.*, 2009; *Gordeev et al.*, 2011] have demonstrated that its CPCP equation given above follows the general behavior of the transpolar potential better than a CPCP equation without the nightside reconnection or viscosity term. Thus, there is good literature support to the equation we use here and to the idea that both reconnection rates contribute to the CPCP and ionospheric convection on the whole. With this knowledge, the application of regression coefficients as contribution factors is a reasonable first step to understand the MI coupling dynamics. This paper determines which type of reconnection controls the CPCP based on the regression coefficients and leaves a detailed analysis of the actual causality for future work. The important caveat is that no prior work has checked the accuracy of the assumed linear relationship between CPCP and the reconnection rates. It is possible, and likely during dynamic transition of the magnetosphere such as compressions, that the contribution of the reconnection rates to CPCP is not linear, but this too is subject for future work. Here we focus on the first-order relationship, and we show that the results are physically realistic.

We fit our model results to $\Phi_{CPCP} = C_D\Phi_D + C_N\Phi_N + \Phi_V$ using a multiple linear regression method and obtain the regression coefficients which give the best fit results. Figure 7 shows the fitting results (green lines) as well as the original transpolar potentials obtained from the OpenGGCM-CTIM model (blue lines), for the 10 January 1997, 30 April 1998, and 12 October 2000 events from top to bottom, respectively. The black vertical lines indicate the pressure front impact on the dayside magnetopause for each event. In each panel, the regression coefficients (C_D and C_N) and the correlation coefficient (CC) between the modeled and fitted CPCPs are shown on the upper left corner for that event. The CC values of three events are 0.828, 0.720, and 0.858, indicating that the CPCP fit function we used provides a realistic representation of the CPCP behavior in the OpenGGCM-CTIM results.

The first solar wind pressure enhancement event occurred on 10 January 1997 during strongly southward IMF. The dayside reconnection coefficient (C_D) is 0.78, about 4 times stronger than the nightside coefficient (C_N). The second event happens on 30 April 1998 while IMF B_z fluctuates around zero, but for the first 2 h of the pressure increase, IMF B_z is mostly weakly southward. For this event, the dayside coefficient is about 2 times higher than the nightside coefficient. These two event studies indicate that dayside reconnection contributes to the CPCP more significantly than nightside reconnection when solar wind pressure enhancement is accompanied by southward IMF. On the other hand, the last event on 12 October 2000 shows a higher nightside regression coefficient, suggesting that the magnetotail reconnection has relatively stronger influence on the CPCP enhancement during northward IMF.

We investigate the physical relationship between the CPCP and the reconnection rates under the different IMF conditions by plotting the ionosphere convection patterns before and after the P_{sw} impact in the left and

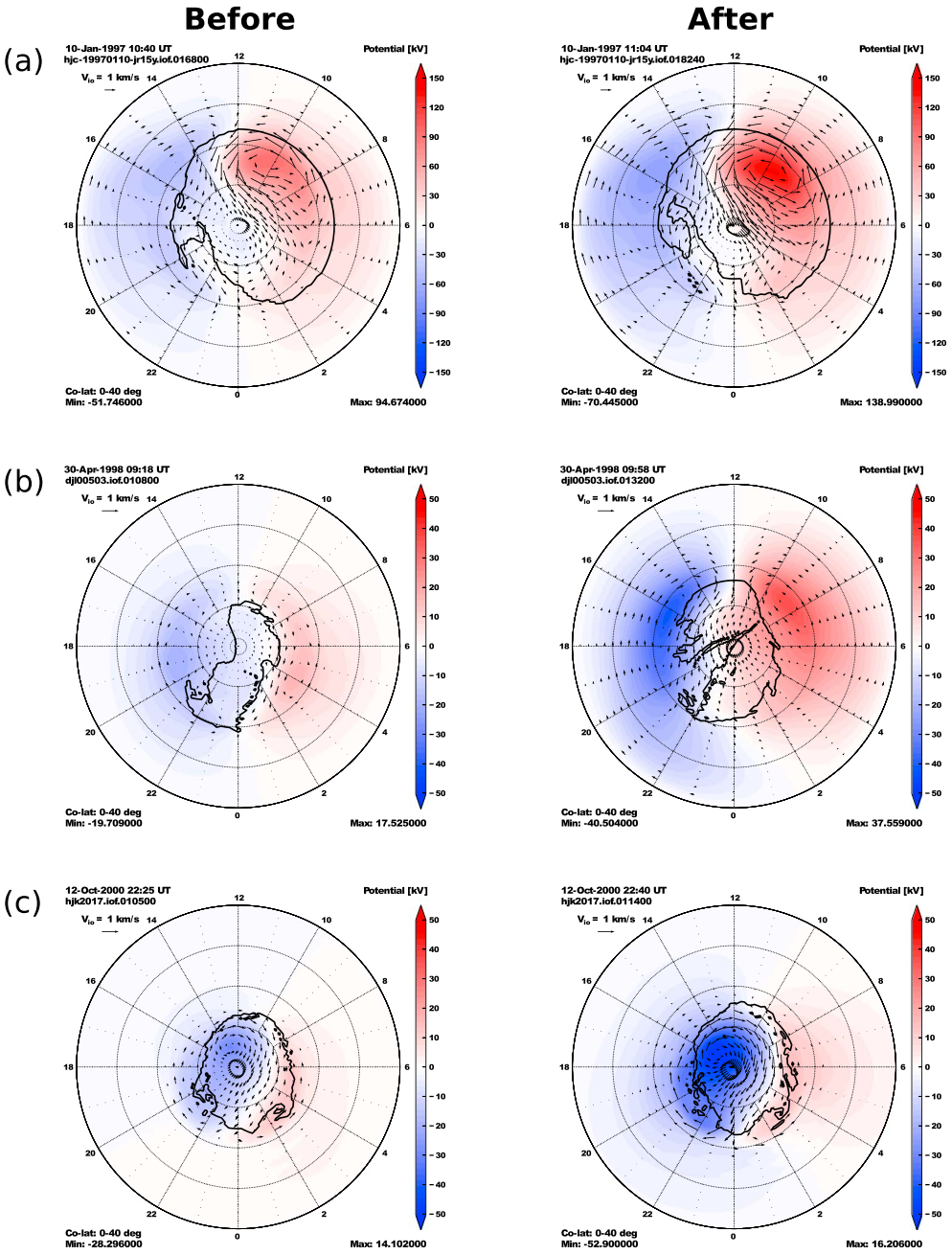

Figure 8. The OpenGGCM-CTIM ionosphere plots before and after the P_{SW} enhancements. The ionospheric conditions on (a) 10 January 1997, (b) 30 April 1998, and (c) 20 October 2000, respectively. The color contour represents electric potentials of the northern ionosphere. The thick black lines and arrows represent the open closed field line boundary and the ionospheric convection vectors.

right columns of Figure 8 for each of the three events. The color contours, arrows, and thick black lines represent electric potentials, plasma flow vectors, and the model determined OCB of the northern ionosphere, respectively. All three events are displayed in Figures 8a–8c, showing that ionospheric potentials and plasma flow speeds intensify after solar wind dynamic pressure increases.

We observe two cell convection patterns for the first two events, as expected from their southward IMF conditions (see the first two columns of Figure 8). When the P_{SW} enhancement intensifies the dayside reconnection rate, we observe strong antisunward plasma flows across the polar cap region. The enhanced ionospheric flows are aligned along a line from 14 to 02 MLT for the 10 January 1997 event and from 12 to 20 MLT

for the 30 April 1998 event. This antisunward plasma convection enhancement and the Earth's dipole magnetic field create the dawn-to-dusk electric fields, which intensifies the typical ionosphere electric field and in turn enhances the transpolar potential.

On 12 October 2000, the northeast IMF condition creates dayside reconnection on the high-latitude, duskside magnetopause. This reconnection produces both sunward and antisunward plasma flows on the dayside ionosphere. The newly merged, kinked open field lines convect sunward due to the magnetic tension force. The ionospheric plasma is frozen-in with these field lines, producing sunward flows in the 13–17 MLT regions (see Figure 8c). These flows create the dusk-to-dawn electric fields, which oppose the typical ionospheric electric fields. As the field lines are drawn away from the reconnection sites, the magnetic tension force reduces and the magnetosheath flow moves the field lines to the antisunward direction. As a result, the ionospheric plasma flows antisunward in 6–12 MLT regions, producing the dawn-to-dusk electric fields. Thus, magnetopause reconnection during northward IMF creates ionospheric convection to both increase and decrease the typical ionospheric electric fields. This weakens the contribution of dayside reconnection on the CPCP. Conversely, intense nightside reconnection during the P_{sw} enhancement produces fast antisunward ionospheric flows near 0 MLT, strengthening the dawn-to-dusk electric field and thus raising the transpolar potential.

This paper has focused on the first-order relation between the CPCP and merging rates as a first step to understand the MI coupling dynamics during sudden enhancements of solar wind dynamic pressure. Although the ECPC model implies a linear response of CPCP to the reconnection rates, previous studies [*Hill et al.*, 1976; *Nagatsuma*, 2002; *Hairston et al.*, 2003] have demonstrated its nonlinear nature by showing that under extreme solar wind conditions, the transpolar potential no longer linearly increases with solar wind driving but saturates instead. However, *Boudouridis et al.* [2004a] have shown that the Hill-Siscoe saturation model [*Siscoe et al.*, 2002] underestimates the transpolar potential for both before and after a sudden P_{sw} enhancement. Thus, modification of existing models is necessary to fill the gap between model and observation. For future work, we will explore the complex behavior of MI dynamics by identifying the parameters responsible for the nonlinear activities and developing the CPCP equation as a function of these parameters.

5. Summary

We investigated where, when, and how solar wind energy flows into the magnetosphere-ionosphere system during sudden enhancements of solar wind dynamic pressure. We specifically focused on the behavior of dayside and nightside reconnection as well as their relative importance on ionospheric convection enhancements by using CPCP as a proxy of the ionospheric convection. From our detailed model analysis, we found the following:

1. Dayside reconnection reacts directly to P_{sw} enhancements and reaches its maximum rate within 9–12 min of the pressure impact. The event study on 10 January 1997 shows that the total magnetosheath field intensifies when the strong P_{sw} compresses the magnetosheath. This initiates stronger antiparallel reconnection on the dayside magnetopause.
2. Nightside reconnection rate reaches its maximum about 13–25 min after the pressure increase. The strong P_{sw} front compresses the magnetotail and increases magnetic field B_x near the central plasma sheet in opposite directions. This intensifies the magnetotail reconnection.
3. For southward IMF, dayside reconnection contributes to CPCP enhancement 2–4 times more than nightside reconnection. On the other hand, for northward IMF, dayside contribution weakens and nightside reconnection has more influence on the CPCP. High-latitude reconnection on the dayside magnetopause under northward IMF produces sunward ionospheric flows, creating a dusk-to-dawn electric field opposing and weakening the typical dawn-to-dusk convection electric field applied to the ionosphere. This leads to a weaker dayside contribution during northward IMF.

Acknowledgments
The simulation data of this paper are available upon request. This work was supported by a grant LBIR# 11RV09COR from the Air Force Office of Scientific Research. We thank C. Y. Huang and Y.-J. Su for useful discussions.

Michael Liemohn thanks Joseph Borovsky and Daniel Welling for their assistance in evaluating this paper.

References

Blanchard, G. T., L. R. Lyons, O. de La Beaujadiere, R. A. Doe, and M. Mendillo (1996), Measurements of the magnetotail reconnection rate, *J. Geophys. Res.*, *101*, 15,265–15,276.

Blanchard, G. T., L. R. Lyons, and J. T. Samson (1997), Accuracy of using the 6300 Å auroral emission to identify the magnetic separatrix on the nightside of the Earth, *J. Geophys. Res.*, *102*, 9697–9703.

Boudouridis, A., E. Zesta, L. R. Lyons, P. C. Anderson, and D. Lummerzheim (2003), Effect of solar wind pressure pulses on the size and strength of the auroral oval, *J. Geophys. Res.*, *108*(A4), 8012, doi:10.1029/2002JA009373.

Boudouridis, A., E. Zesta, L. R. Lyons, and P. C. Anderson (2004a), Evaluation of the Hill-Siscoe transpolar potential saturation model during a solar wind dynamic pressure pulse, *Geophys. Res. Lett.*, *31*, L23802, doi:10.1029/2004GL021252.
Boudouridis, A., E. Zesta, L. R. Lyons, P. C. Anderson, and D. Lummerzheim (2004b), Magnetospheric reconnection driven by solar wind pressure fronts, *Ann. Geophys.*, *22*, 1367–1378.
Boudouridis, A., E. Zesta, L. R. Lyons, P. C. Anderson, and D. Lummerzheim (2005), Enhanced solar wind geoeffectiveness after a sudden increase in dynamic pressure during southward IMF orientation, *J. Geophys. Res.*, *110*, A05214, doi:10.1029/2004JA010704.
Boudouridis, A., L. R. Lyons, E. Zesta, and J. M. Ruohoniemi (2007), Dayside reconnection enhancement resulting from a solar wind dynamic pressure increase, *J. Geophys. Res.*, *112*, A06201, doi:10.1029/2006JA012141.
Boudouridis, A., L. R. Lyons, E. Zesta, J. M. Ruohoniemi, and D. Lummerzheim (2008a), Nightside flow enhancement associated with solar wind dynamic pressure driven reconnection, *J. Geophys. Res.*, *113*, A12211, doi:10.1029/2008JA013489.
Boudouridis, A., E. Zesta, L. R. Lyons, P. C. Anderson, and A. J. Ridley (2008b), Temporal evolution of the transpolar potential after a sharp enhancement in solar wind dynamic pressure, *Geophys. Res. Lett.*, *35*, L02101, doi:10.1029/2007GL031766.
Boudouridis, A., L. R. Lyons, E. Zesta, J. M. Weygand, A. J. Ribeiro, and J. M. Ruohoniemi (2011), Statistical study of the effect of solar wind dynamic pressure fronts on the dayside and nightside ionospheric convection, *J. Geophys. Res.*, *116*, A10233, doi:10.1029/2011JA016582.
Boyle, C., P. H. Reiff, and M. Hairston (1997), Empirical polar cap potentials, *J. Geophys. Res.*, *102*(A1), 111–126.
Bristow, W. A., R. A. Greenwald, S. G. Shepherd, and J. M. Hughes (2004), On the observed variability of the cross-polar cap potential, *J. Geophys. Res.*, *109*, A02203, doi:10.1029/2003JA010206.
de La Beaujardiere, O., L. R. Lyons, and E. Friis-Christensen (1991), Sondrestrom radar measurements of the reconnection electric field, *J. Geophys. Res.*, *96*, 13,907–13,912.
Dorelli, J. C., M. Hesse, M. M. Kuznetsova, L. Rastaetter, and J. Raeder (2004), A new look at driven magnetic reconnection at the terrestrial solar magnetopause, *J. Geophys. Res.*, *109*, A12216, doi:10.1029/2004JA010458.
Fuller-Rowell, T. J., D. Rees, S. Quegan, R. J. Moffett, M. V. Codrescu, and G. H. Millward (1996), A coupled thermosphere-ionosphere model (CTIM), in *STEP Report*, edited by R. W. Schunk, 217 pp., NOAA/NGDC, Scientific Committee on Solar Terrestrial Physics (SCOSTEP), Boulder, Colo.
Gordeev, E. I., V. A. Sergeev, T. I. Pulkkinen, and M. Palmroth (2011), Contribution of magnetotail reconnection to the cross-polar cap electric potential drop, *J. Geophys. Res.*, *116*, A08219, doi:10.1029/2011JA016609.
Hairston, M. R., T. W. Hill, and R. A. Heelis (2003), Observed saturation of the ionospheric polar cap potential during the 31 March 2001 storm, *Geophys. Res. Lett. 30*(6), 1325, doi:10.1029/2002GL015894.
Hill, T. W., A. J. Dessler, and R. A. Wolf (1976), Mercury and Mars: The role of ionospheric conductivity in the acceleration of magnetospheric particles, *Geophys. Res. Lett.*, *3*, 429–432.
Hubert, B., S. E. Milan, A. Grocott, C. Blockx, S. W. H. Cowley, and J.-C. Gerard (2006a), Dayside and nightside reconnection rates inferred from IMAGE FUV and Super Dul Auroral Radar Network data, *J. Geophys. Res.*, *111*, A03217, doi:10.1029/2005JA011140.
Hubert, B., M. Palmroth, T. V. Laitinen, P. Janhunen, S. E. Milan, A. Grocott, S. W. H. Cowley, T. Pulkkinen, and J.-C. Gerard (2006b), Compression of the Earth's magnetotail by interplanetary shocks directly drives transient magnetic flux closure, *Geophys. Res. Lett.*, *33*, L10105, doi:10.1029/2006GL026008.
Hubert, B., C. Blockx, S. E. Milan, and S. W. H. Cowley (2009), Statistical properties of flux closure induced by solar wind dynamic pressure fronts, *J. Geophys. Res.*, *114*, A07211, doi:10.1029/2008JA013813.
Kihn, E. A., R. Redmon, A. J. Ridley, and M. R. Hairston (2006), A statistical comparison of the AMIE derived and DMSPSSIES observed high-latitude ionospheric electric field, *J. Geophys. Res.*, *111*, A08303, doi:10.1029/2005JA011310.
Knipp, D. J., and B. A. Emery (1997), Mapping ionospheric substorm response, *Adv. Space Res.*, *20*(4/5), 895–905.
Lockwood, M. (1991), On flow reversal boundaries and transpolar voltage in average models of high latitude convection, *Planet. Space Sci.*, *39*, 397–409.
Lockwood, M., and S. W. H. Cowley (1992), Ionospheric convection and the substorm cycle, in *Substorms 1*, *Proceedings of the First International Conference on Substorms, ICS-1*, edited by C. Mattock, ESASP-335, pp. 99–109, Eur. Space Agency Publ, Noordvijk, Netherlands.
Lockwood, M., M. Hairston, I. Finch, and A. Rouillard (2009), Transpolar voltage and polar cap flux during the substorm cycle and steady convection events, *J. Geophys. Res.*, *114*, A01210, doi:10.1029/2008JA013697.
Lyons, L. R., E. Zesta, J. C. Samson, and G. D. Reeves (2000), Auroral disturbances during the January 10, 1997 magnetic storm, *Geophys. Res. Lett.*, *27*, 3237–3240.
Milan, S. E. (2004), Dayside and nightside contributions to the cross polar cap potential: Placing an upper limit on a viscous-like interaction, *Ann. Geophys.*, *22*(10), 3771–3777.
Milan, S. E., S. W. H. Cowley, M. Lester, D. M. Wright, J. A. Slavin, M. Fillingim, C. W. Carlson, and H. J. Singer (2004), Response of the magnetotail to changes in the open flux content of the magnetosphere, *J. Geophys. Res.*, *109*, A04220, doi:10.1029/2003JA010350.
Milan, S. E., G. Provan, and B. Hubert (2007), Magnetic flux transport in the Dungey cycle: A survey of dayside and nightside reconnection rates, *J. Geophys. Res.*, *112*, A01209, doi:10.1029/2006JA011642.
Milan, S. E., J. Hutchinson, P. D. Boakes, and B. Hubert (2009), Influences on the radius of the auroral oval, *Ann. Geophys.*, *27*, 2913–2924.
Nagatsuma, T. (2002), Saturation of polar cap potential by intense solar wind electric fields, *Geophys. Res. Lett.*, *29*(10), 1422, doi:10.1029/2001GL014202.
Ober, D. M., N. C. Maynard, W. J. Burke, W. K. Peterson, J. B. Sigwarth, L. A. Frank, J. D. Scudder, W. J. Hughes, and C. T. Russell (2001), Electrodynamics of the poleward auroral border observed by Polar during a substorm on April 22, 1998, *J. Geophys. Res.*, *106*(A4), 5927–5943.
Ober, D. M., G. R. Wilson, N. C. Maynard, W. J. Burke, and K. D. Siebert (2006), MHD simulation of the transpolar potential after a solar-wind density pulse, *Geophys. Res. Lett.*, *33*, L04106, doi:10.1029/2005GL024655.
Ober, D. M., G. R. Wilson, W. J. Burke, N. C. Maynard, and K. D. Siebert (2007), Magnetohydrodynamic simulations of transient transpolar potential responses to solar wind density changes, *J. Geophys. Res.*, *112*, A10212, doi:10.1029/2006JA012169.
Østgaard, N., J. Moen, S. B. Mende, H. U. Frey, T. J. Immel, P. Gallop, K. Oksavik, and M. Fujimoto (2005), Estimates of magnetospheric reconnection rate based on IMAGE-FUV and EISCAT measurements, *Ann. Geophys.*, *23*, 123.
Parker, E. N. (1973), Comments on the reconnection rate of magnetic fields, *J. Plasma Phys.*, *9*, 49–63.
Raeder, J. (2003), Global magnetohydrodynamics—A tutorial, in *Space Plasma Simulation*, *Lecture Notes in Physics*, edited by J. Buechner, C. T. Dum, and M. Scholer, 615 pp., Springer-Verlag, Heidelberg, Germany.
Raeder, J. (2005), Polar cap potential saturation during large geomagnetic storms, *Adv. Space Res.*, *36*, 1804–1808.
Raeder, J., J. Berchem, and M. Ashour-Abdalla (1998), GGCM modeling of ionospheric convection: The GEM grand challenge, *J. Geophys. Res.*, *103*, 14,787–14,797.

Raeder, J., Y. Wang, and T. Fuller-Rowell (2001), Geomagnetic storm simulation with a coupled magnetosphere-ionosphere-thermosphere model, in *Space Weather: Progress and Challenges in Research and Applications*, *Geophys. Monogr. Ser.*, vol. 125, edited by P. Song, H. J. Singer, and G. Siscoe, pp. 377–384, AGU, Washington, D. C.

Raeder, J., D. Larson, W. Li, E. L. Kepko, and T. Fuller-Rowell (2008), OpenGGCM simulations for the THEMIS mission, *Space Sci. Rev.*, *141*, 535–555, doi:10.1007/s11214-0421-5.

Reiff, P. H., R. R. Spiro, and T. Hill (1981), Dependence of polar cap potential on interplanetary parameters, *J. Geophys. Res.*, *86*(A9), 7639–7648.

Siscoe, G. L., G. M. Erickson, B. U. O. Sonnerup, N. C. Maynard, J. A. Schoendorf, K. D. Siebert, D. R. Weimer, W. W. White, and G. R. Wilson (2002), Hill model of transpolar potential saturation: Comparisons with MHD simulations, *J. Geophys. Res.*, *107*(A6), 1075, doi:10.1029/2001JA000109.

Slinker, S. P., J. A. Fedder, B. A. Emery, K. B. Baker, D. Lummerzheim, J. G. Lyon, and F. J. Rich (1999), Comparison of global MHD simulations with AMIE simulations for the events of May 19–20, 1996, *J. Geophys. Res.*, *104*(A12), 28,379–28,395, doi:10.1029/1999JA900403.

Sonnerup, B. U. O. (1988), On the theory of steady state reconnection, *Comput. Phys. Commun.*, *49*, 143–159.

Vasyliunas, V. M. (1970), Mathematical models of magnetospheric convection and its coupling to the ionosphere in *Particles and Fields in the Magnetosphere*, 61 pp., D. Reidel, Dordrecht, Netherlands.

Wolf, R. A. (1975), Effects of ionospheric conductivity on convective flow of plasma in the magnetosphere, *J. Geophys. Res.*, *75*, 4677–4698.

Wolf, R. A. (1983), The quasi-static (slow flow) region of the magnetosphere, in *Solar Terrestrial Physics*, edited by R. L. Carovillano and J. M. Forbes, pp. 303–368, D. Reidel, Hingham, Mass.

Zesta, E., H. J. Singer, D. Lummerzheim, C. T. Russell, L. R. Lyons, and M. J. Brittnacher (2000), The effect of the January 10, 1997, pressure pulse on the magnetosphere-ionosphere current system, in *Magnetospheric Current Systems*, *Geophys. Monogr. Ser.*, vol. 118, edited by S. Ohtani et al., pp. 217–226, AGU, Washington, D. C.